Large MIMO sonar systems:
a tool for underwater surveillance

Yan Pailhas, Yvan Petillot

Ocean Systems Laboratory

Heriot Watt University

Edinburgh, UK, EH14 4AS

Email: Y.Pailhas@hw.ac.uk

Abstract—**Multiple Input Multiple Output sonar systems offer new perspectives for target detection and underwater surveillance. In this paper we present an unified formulation for sonar MIMO systems and study their properties in terms of target recognition and imaging. Here we are interested in large MIMO systems. The multiplication of the number of transmitters and receivers non only provides a greater variety in term of target view angles but provides also in a single shot meaningful statistics on the target itself. We demonstrate that using large MIMO sonar systems and with a single shot it is possible to perform automatic target recognition and also to achieve super-resolution imaging. Assuming the view independence between the MIMO pairs the speckle can be solved and individual scatterers within one resolution cell decorelate. A realistic 3D MIMO sonar simulator is also presented. The output of this simulator will demonstrate the theoretical results.**

I. INTRODUCTION

MIMO stands for Multiple Input Multiple Output. It refers to a structure with spatially spaced transmitters and receivers. It has been widely investigated during the last two decades for wireless communications mainly to overcome the multipath problem in complex environments (principally urban environment). MIMO systems have received a lot of interest in recent years in the radar community [1], [2].

Multiple Input Multiple Output sonar systems have raised a lot of interest during the recent years mainly in the ASW (anti-submarine warfare) community. Often referred as multistatic sonars they overcome monostatic sonar systems in target localisation [3] and detection performances [4]. CMRE (Centre for Maritime Research and Experimentation) in particular developed a deployable low frequency multi-static sonar system called DEMUS and conducted a series of trials including pre-DEMUS06 and SEABAR07.The DEMUS hardware consists of one source and three receiver buoys and can be denominated as a SIMO (Single Input Multiple Output) system. A lot of the efforts were then focussed on the data fusion and the target tracking problems.

In this paper we focus our attention on large MIMO sonar systems. We will show that having a greater variety of views of the scene offers meaningful statistics on targets with a single snapshot and therefore have interest in automatic target recognition. Having more views on a particular scene or target also poses the problem of merging them. We will demonstrate that with enough views one can solve the speckle noise and then use the multi-view to produce super-resolution MIMO images.

This paper is organised as follows: In section II we present the radar MIMO formulation and derive the broadband sonar MIMO expression. We then present a realistic 3D MIMO simulator. In section IV we demonstrate some of the MIMO sonar capabilities: target recognition and super resolution.

II. REFORMULATION OF THE BROADBAND MIMO SONAR PROBLEM

A. The RADAR formulation

The first formulation for surveillance MIMO systems has been made by the radar community [1]. The MIMO system model can usually be expressed by: $\bar{r} = \overline{H}.\bar{s} + \bar{n}$, where $\bar{r}$ represents the receivers, $\bar{s}$ the transmitters, $\bar{n}$ the noise, and $\overline{H}$ the channel matrix. The channel matrix include the wave propagation in the medium from any transmitters to any receivers and the target reflection. At first, targets were represented using the "point target" assumption [5]. Since then, several target models have been proposed such as rectangular-shape target in [2] composed of an infinite number of scatterers. We present here the most popular model for a radar target model which is the finite scatterer model [6].

In [6] the authors formulate narrowband MIMO radar using a finite point target model. A target is represented here with Q scattering points spatially distributed. Let $\{X_q\}_{q\in[1,Q]}$ be their locations. The reflectivity of each scattering point is represented by the complex random variable ζ_q. All the ζ_q are assumed to be zero-mean, independent and identically distributed with a variance of $E[|\zeta_q|^2] = 1/Q$. Let Σ be the reflectivity matrix of the target, $\Sigma = \mathrm{diag}(\zeta_1, ..., \zeta_Q)$. By using this notation the average RCS (radar cross section) of the target $\{X_q\}$, $E[\mathrm{tr}(\Sigma\Sigma^H)]$, is normalised to 1.

The MIMO system comprises a set of K transmitters and L receivers. Each transmitter k sends a pulse $\sqrt{E/K}.s_k(t)$. We assume that all the pulses $s_k(t)$ are normalised. Then E represents the total transmit energy of the MIMO system. Receiver l receives from transmitter k the signal $z_{lk}(t)$ which can be written as:

$$z_{lk}(t) = \sqrt{\frac{E}{K}} \sum_{q=1}^{Q} h_{lk}^{(q)} s_k \left(t - \tau_{tk}(X_q) - \tau_{rl}(X_q)\right) \quad (1)$$

with $h_{lk}^{(q)} = \zeta_q \exp\left(-j2\pi f_c[\tau_{tk}(X_q) + \tau_{rl}(X_q)]\right)$ (2)

where f_c is carrier frequency, $\tau_{tk}(X_q)$ represents the propagation time delay between the transmitter k and the scattering

point X_q, $\tau_{rl}(X_q)$ represents the propagation time delay between the scattering point X_q and the receiver l. Note that $h_{lk}^{(q)}$ represents the total phase shift due to the propagation from the transmitter k to the scattering point X_q, the propagation from the scattering point X_q to the receiver l and the reflection on the scattering point X_q.

Assuming the Q scattering points are close together (*i.e.* within a resolution cell), we can write:

$$
\begin{aligned}
s_k\left(t - \tau_{tk}(X_q) - \tau_{rl}(X_q)\right) &\approx s_k\left(t - \tau_{tk}(X_0) - \tau_{rl}(X_0)\right) \\
&= s_k^l(t, X_0)
\end{aligned} \tag{3}
$$

where X_0 is the centre of gravity of the target $\{X_q\}$. So Eq. (1) becomes:

$$
\begin{aligned}
z_{lk}(t) &= \sqrt{\frac{E}{K}} s_k^l(t, X_0) \times \\
&\quad \left(\sum_{q=1}^{Q} \zeta_q \exp\left(-j2\pi f_c[\tau_{tk}(X_q) + \tau_{rl}(X_q)]\right)\right) \\
&= \sqrt{\frac{E}{K}} \left(\sum_{q=1}^{Q} h_{lk}^{(q)}\right) s_k^l(t, X_0)
\end{aligned} \tag{4}
$$

B. The MIMO sonar extension

In this section we propose a reformulation of the Haimovich model presented in section II-A to suit broadband sonar systems. We demonstrate in previous works [7] that for broadband sonar a formulation in the Fourier domain is more appropriate. Eq. (1) becomes:

$$
Z_{lk}(\omega) = \sqrt{\frac{E}{K}} \sum_{q=1}^{Q} h_{lk}^{(q)} S_k(\omega) \mathbf{e}^{-j\omega[\tau_{tk}(X_q) + \tau_{rl}(X_q)]} \tag{5}
$$

Using the following notations:

$$
\begin{aligned}
\tau_{tk}(X_q) &= \tau_{tk}(X_0) + \tilde{\tau}_{tk}(X_q) \\
\tau_{rl}(X_q) &= \tau_{rl}(X_0) + \tilde{\tau}_{tk}(X_q)
\end{aligned} \tag{6}
$$

and

$$
H_{lk}(X_0, \omega) = \sqrt{\frac{E}{K}} . \mathbf{e}^{-j(2\pi f_c + \omega).[\tau_{tk}(X_0) + \tau_{rl}(X_0)]} \tag{7}
$$

the following expression can be derived:

$$
\begin{aligned}
Z_{lk}(\omega) &= H_{lk}(X_0, \omega) \left(\sum_{q=1}^{Q} \tilde{h}_{lk}^{(q)} \mathbf{e}^{-j\omega[\tilde{\tau}_{tk}(X_q) + \tilde{\tau}_{rl}(X_q)]}\right) S_k(\omega) \\
&= H_{lk}(X_0, \omega) F_{\infty}(\omega, \theta_l, \phi_k) S_k(\omega)
\end{aligned} \tag{8}
$$

where θ_l is the angle of view of the target from the transmitter and ϕ_k is the angle of view of the target from the receiver.

Eq. (8) can be interpreted as follows: the first term corresponds to the propagation of the wave to and from the target, the second term is the form function of the target, the third term is the transmitted signal. The main advantage of this formulation is the clear separation between propagation terms and target reflection terms. In our formulation the target form function F_{∞} is independent of any particular model. One can use point scatterer models or more complex ones.

III. MIMO SIMULATOR

In this section we describe the main components of the 3D MIMO sonar simulator.

A. Seabed interface

To model the seabed interface we generate 2D fractional Brownian motion (fBm) using the Incremental Fourier Synthesis Method developed by Kaplan and Kuo [8]. The main idea is to model the 1st and 2nd order increments I_x, I_y and I_2. I_2 for example is given by:

$$
\begin{aligned}
I_2(m_x, m_y) = \quad & B(m_x + 1, m_y + 1) + B(m_x, m_y) \\
& - B(m_x, m_y + 1) - B(m_x, m_y + 1)
\end{aligned}
$$

where B is the 2D fBm. Those 1st and 2nd order increments can be computed thanks to their FFTs. The 2nd order increment FFT is given by:

$$
S_2(\omega_x, \omega_y) = \frac{32\sqrt{\pi} \sin^2(\omega_x/2) \sin^2(\omega_y/2) \Gamma(2H+1) \sin(\pi H)}{\sqrt{\omega_x^2 + \omega_y^2}^{2H+2}} \tag{9}
$$

where H is the Hurst parameter. Figure 1 displays an example of 2D fBm surface generated using this technique.
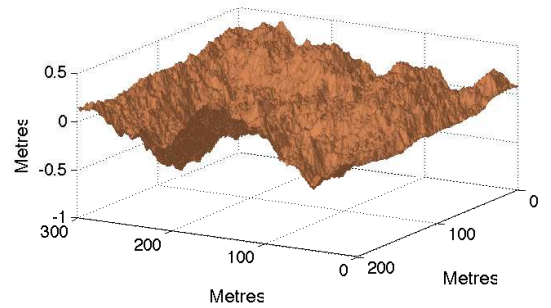

Fig. 1.   Example of 2D fBm with H = 0.8 (fractal dimension = 2.2)

B. Bistatic reverberation level

The bistatic scattering strength is computed using the model developed by Williams and Jackson [9]. It is given by:

$$
S_b(\theta_s, \phi_s, \theta_i) = 10\log[\sigma_{br}(\theta_s, \phi_s, \theta_i) + \sigma_{bv}(\theta_s, \phi_s, \theta_i)] \tag{10}
$$

where $\sigma_{br} = [\sigma_{kr}^\eta + \sigma_{pr}^\eta]^{1/\eta}$ is the bistatic roughness scattering which includes the Kirchhoff approximation and the perturbation approximation. σ_{bv} is the sediment bistatic volume scattering. S_b depends on the bistatic geometry as well as the sediment physical properties. Figure 2 displays the bistatic scattering strength for a Tx/Rx pair situated 141m apart and both at 7.5m from the seafloor. The S_b is computed for two different sediment types (coarse sand and sandy mud) for the same fBm interface.

C. Propagation

Sound propagation in shallow water can become extremely complex. Because we are modelling very shallow water environment we assume a constant sound speed through the water column. To model the multipath we are using the mirror theorem. We use ray tracing techniques to compute the different propagation paths. The simulations done in this paper consider a maximum of three bounces.

To synthesise time echo a random scatterer point cloud including random position and random intensity is generated
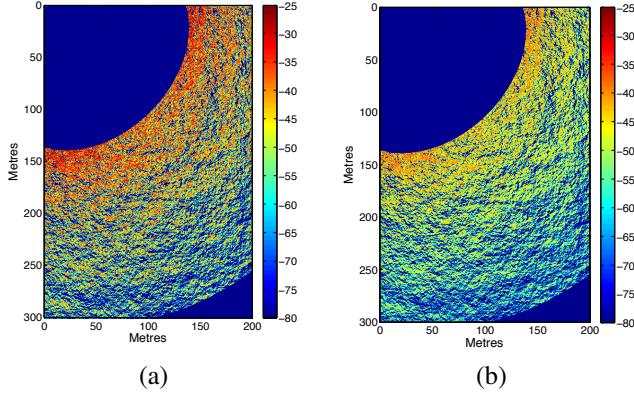
Fig. 2. Bistatic scattering strength relative to one Tx located at [0m,100m] and a Rx located at [100m,0m] for (a) a coarse sand sediment type and (b) a sandy mud sediment type.

for each cell in the seabed. Note that once the point cloud is generated, it can be saved for other simulations with the same configuration.

To synthesise the MIMO echoes from a 200m × 300m scene with 50cm cell resolution we have to compute 400 × 600 cells × 20 scatterers per cell × 100 MIMO pairs different paths which represents around half a billion paths (direct paths only). Brute force computation using MatLab on a standard laptop requires around 2 months of computation. This can be drastically reduced by analysing the properties of propagation in water and the circular convolution properties of the DFT. The main tool to propagate a signal is free water is the well known FFT property: $f(t - u) \Leftrightarrow e^{-iu\omega} \hat{f}(\omega)$. If we consider the echo related to one cell, this echo is extremely sparse over a 600m range signal. The idea is to compute the propagated signal over a much smaller window. Figure 3 draws the outlines of the algorithm: the full scene is divided into range bands, on Fig. 3(a) each colour band represents a 10m range division. The echoes relative to each band are computed independently on a small window of 20m (cf. figure 3(b)). The echoes are then recombined to give the full range bistatic response as seen in figure 3(c). Using those techniques greatly reduces the computation time from 2 months to around 10 hours.

IV. LARGE MIMO SYSTEMS PROPERTIES

In this section we discuss the properties of large MIMO sonar systems.

A. Incoherent MIMO target snapshot

Back to the results of section II we are interested in the MIMO intensity response of an object. It is interesting to note that the term $\sum_{q=1}^{Q} h_{lk}^{(q)}$ in Eq. (4) corresponds in essence to a random walk in the complex plane where each step $h_{lk}^{(q)}$ can be modelled by a random variable.

Lets assume that the reflectivity coefficients ζ_q can be modelled by the random variable $\frac{1}{\sqrt{Q}} e^{2i\pi U}$ where $U \in [0,1]$ is the uniform distribution. This hypothesis implies that:

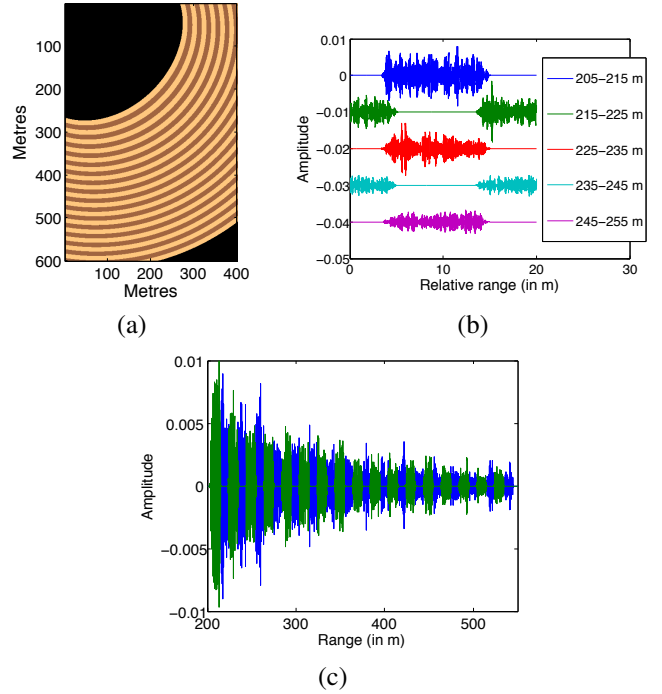$$h_{lk}^{(q)} = \frac{1}{\sqrt{Q}} e^{2i\pi U} \qquad (11)$$

Fig. 3. (a) of the observed scene in 10m range band. (b) Individual range band echo contribution. (c) Full echo response recomposition.

Thanks to the central limit theorem we can write:

$$\lim_{Q \to +\infty} \sqrt{\left| \sum_{q=1}^{Q} h_{lk}^{(q)} \right|^2} = \text{Rayleigh}(1/\sqrt{2}) \qquad (12)$$

However the central limit theorem gives only the asymptotic behaviour of the random variable. As the number of scattering points becomes large the reflectivity of the target can be modelled by a Rayleigh distribution.

The convergence of Eq. (12) however is fast as shown in [10]. Figure 4 shows the convergence of the reflectivity PDF of a Q scattering points target. As this figure shows, for $Q \geq 5$ the reflectivity PDF matches closely the Rayleigh$(1/\sqrt{2})$ probability distribution. In Fig. 4 we can see that the probability function of the 100 scatterer target and Rayleigh$(1/\sqrt{2})$ are almost indistinguishable.
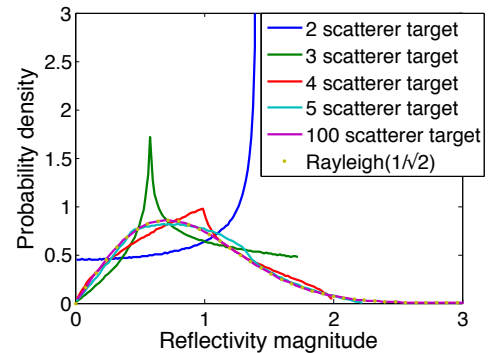

Fig. 4. Reflectivity probability density functions of a Q scattering points target with $Q = 2, 3, 4, 5$ & 100 using the scatterer reflectivity model from Eq. (11).

Here we want to take advantage of the dissimilarities of the probability density functions to estimate the number of scattering points. Each observation is a realisation of the random variable $\gamma_n = \sqrt{\left|\sum_{q=1}^{Q} h_{lk}^{(q)}\right|^2}$ with Q the number of scattering points. Each set of observations $\Gamma = \{\gamma_n\}_{n\in[1,N]}$ where N is the number of views represents the MIMO output.

Given a set of observations Γ we can compute the probability that the target has Q scatterers using Bayes rules:

$$P(T_Q|\Gamma) = \frac{P(\Gamma|T_Q)P(T_Q)}{P(\Gamma)} \tag{13}$$

where T_Q represents the event that the target has Q scatterers. Assuming the independence of the observations $P(\Gamma|T_Q)$ can be written as:

$$P(\Gamma|T_Q) = \prod_{n=1}^{N} P(\gamma_n|T_Q) \tag{14}$$

$P(\gamma_n|T_Q)$ is computed thanks to the reflectivity density function presented in Fig. 4. We consider 4 target types: 2 scatterer target, 3 scatterer target, 4 scatterer target and 5+ scatterer target. So $Q \in \{2, 3, 4, 5+\}$. Therefore we can write:

$$P(\Gamma) = \sum_{Q=2}^{5} P(\Gamma|T_Q)P(T_Q) \tag{15}$$

Given that we have no *a priori* information about the target we can assume that $P(T_Q)$ is equal for all target class T_Q. Eq. (13) then becomes:

$$P(T_Q|\Gamma) = \frac{\prod_{n=1}^{N} P(\gamma_n|T_Q)}{\sum_{Q=2}^{5+} P(\Gamma|T_Q)} \tag{16}$$

The estimated target class corresponds to the class which maximises the conditional probability given by Eq. (16).
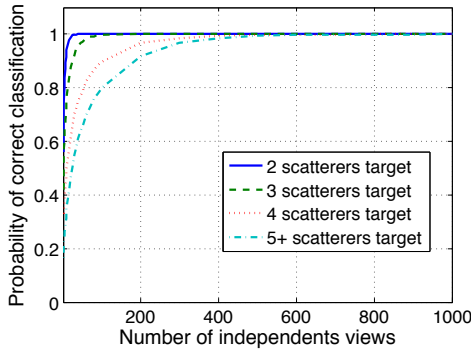

Fig. 5. Correct classification probability against the number of independent views for 4 classes of targets (2, 3, 4 and 5+ scattering points targets).

To validate the theory, a number of experiments have been run in simulation. For each number of views 10^6 classification tests have been computed. Note that the simulations have been run with 10 dB SNR. Fig. 5 draws the probability of correct classification for each class depending on the number of views. The first observation we can make is that it is possible to estimate the number of scattering points in a target if the number of scatterers is low (≤ 4). The 2 scattering point target can be seen as a dipole and its reflectivity PDF

differs considerably from any n scattering points target (with $n > 2$). For this reason fewer independent views are needed to correctly classify this class of target. With only 10 views, a 2 scattering point target is correctly classified in 96% of cases.

B. Super-resolution MIMO imaging

Let $r_l(t)$ be the total received signal at the receiver l. According to our previous notations we have for $l \in [1, L]$:

$$r_l(t) = \sum_{k=1}^{K} z_{lk}(t) \tag{17}$$

where $z_{lk}(t)$ has been defined in Eq. (4). Let x_{lk} output of r_l from the filter bank $s_k^*(t)$ with $k \in [1, K]$. Assuming orthogonal output pulses we have:

$$x_{lk} = r_l \star s_k^*(t) = \sum_{q=1}^{Q} h_{lk}^{(q)} \tag{18}$$

Approaching the data fusion problem from the detection problem perspective, we can choose the following detection rule which represents the average target echo intensity from all the bistatic views:

$$\mathcal{F}(\mathbf{r}) = \frac{1}{N} \sum_{l,k} ||x_{lk}||^2 \tag{19}$$

Using the same target probability distribution stated in the model presented earlier, we deduce that $\mathcal{F}(\mathbf{r})$ follows the probability distribution:

$$\mathcal{F}(\mathbf{r}) \sim \frac{1}{N} \sum_{n=1}^{N} \text{Rayleigh}^2(\sigma) \tag{20}$$

Using the properties of the Rayleigh distribution we can write:

$$\sum_{n=1}^{N} \text{Rayleigh}^2(\sigma) \sim \Gamma(N, 2\sigma^2) \tag{21}$$

where Γ is the Gamma distribution. So the PDF of the detection rule $\mathcal{F}(\mathbf{r})$ is $N.\Gamma(Nx, N, 1)$. The asymptotic behaviour of the detection rule $\mathcal{F}(\mathbf{r})$ can be deduced from the following identity [11]:

$$\lim_{N\to+\infty} N.\Gamma(Nx, N, 1) = \delta(1-x) \tag{22}$$

Eq. 22 shows that the detection rule $\mathcal{F}(\mathbf{r})$ converges toward the RCS defined in section II-A which means that the scatterers within one resolution cell decorrelate between each other. MIMO systems then solve the speckle noise in the target response. This demonstrates why super-resolution can be achieved with large MIMO systems.

In order to image the output of the MIMO system we will use the multi-static back-projection algorithm which is a variant of the bistatic back-projection algorithm developed by the Synthetic Aperture Radar (SAR) community. Further details can be found in [12]. Using the back-projection algorithm the Synthetic Aperture Sonar (SAS) image is computed by integrating the echo signal along a parabola. In the bistatic case the integration is done along ellipses. For the multi-static scenario the continuous integration is replaced by a finite sum in which each term corresponds to one transmitter/receiver pair contribution.

In the following simulation we aim to demonstrate that we can recover the geometry of a target (*i.e.* the location of its scatterers). We chose a "L" shape MIMO configuration. The transmitters are placed in the x-axis, the receivers are on the y-axis. The MIMO system frequency band is 50 kHz to 150 kHz. We consider a 3 point scatterers target, the scatterers are separated by one wavelength.
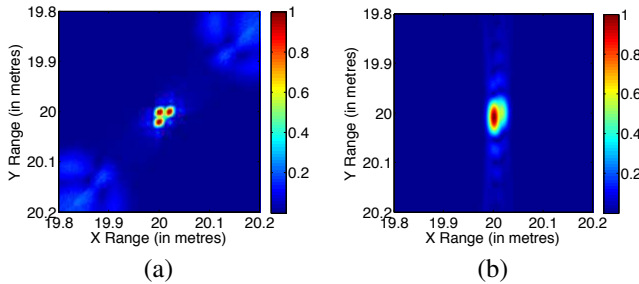

Fig. 6. 3 scatterers target: (a) MIMO image using 10 transmitters and 10 receivers with 3 metres spacing, (b) SAS image.

In figure 6(a) we consider a 10 Tx × 10 Rx MIMO system. With this configuration we are able to clearly image the 3 scatterer target in so doing achieve super resolution imaging. For comparison purposes we have computed the SAS image (cf. Fig. 6(b)) of the same target using the same frequency band and at the same range. The full geometry of the target is not recovered there.

Figure 7 displays a synthetic aperture MIMO image of a realistic environment: the background is a fractal coarse sand seafloor, a mid-water target is present at the location [200m, 150m].
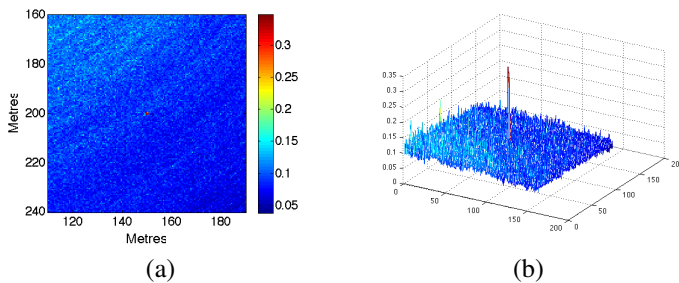

Fig. 7. Synthetic aperture MIMO image of a mid water -30dB target on a coarse sand sediment background, (a) 2D image, (b) 3D image.

Synthetic aperture MIMO imaging shares a lot of features with standard SAS imaging. In particular the image is projected onto a plane or a bathymetry estimate. The image of a mid water target will then appear unfocused for this particular projection. By moving the projection plane through the water column the MIMO target image will focus at its actual depth. Using simple autofocus algorithm it is then possible to estimate the depth of the target even if the MIMO system is coplanar. For a mid water target at 400m range in a 15m depth environment it is possible to estimate its depth with 10 to 50 cm accuracy. Figure 8 displays the autofocus results and the estimated target depth compared with the ground truth.
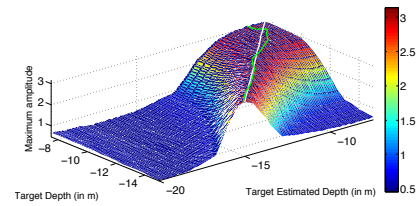

Fig. 8. Autofocus algorithm results based on maximising the scattering response: ground truth (white curve) and estimated depth (green curve).

V. CONCLUSION

In this paper we have posed the fundamental principles for MIMO sonar systems. We propose a new formulation for broadband MIMO sonar systems by separating clearly the terms of propagation and the terms of target reflection. We show the recognition and the super-resolution imaging capabilities of such systems and present a realistic 3D MIMO simulator. The MIMO sonar capabilities described in this paper make such a system a very attractive tool for underwater surveillance.

REFERENCES

[1] D. Bliss and K. Forsythe, "Multiple-input multiple-output (mimo) radar and imaging: Degrees of freedom and resolution," in *Proc. 37th Asilomar Conf. Signals, Systems and Computers*, 2003.

[2] E. Fishler, A. Haimovich, R. Blum, J. Cimini, L.J., D. Chizhik, and R. Valenzuela, "Spatial diversity in radars-models and detection performance," *Signal Processing, IEEE Transactions on*, vol. 54, no. 3, pp. 823–838, March 2006.

[3] S. Kim, B. Ku, W. Hong, and H. Ko, "Performance comparison of target localization for active sonar systems," *Aerospace and Electronic Systems, IEEE Transactions on*, vol. 44, no. 4, pp. 1371–1380, 2008.

[4] M. Fewell and S. Ozols, "Simple detection-performance analysis of multistatic sonar for anti-submarine warfare," DSTO Defence Science and Technology Organisation, Tech. Rep., 2011.

[5] M. Skolnik, *Introduction to Radar Systems*. Mc-Graw-Hill, 2002.

[6] A. Haimovich, R. Blum, and L. Cimini, "Mimo radar with widely separated antennas," *Signal Processing Magazine, IEEE*, vol. 25, no. 1, pp. 116–129, 2008.

[7] Y. Pailhas, C. Capus, K. Brown, and P. Moore, "Measured target responses to bio-inspired sonar pulses," in *Proceedings of the 8th European Conference on Underwater Acoustics, ECUA 06*, 2006.

[8] L. Kaplan and C.-C. Kuo, "An improved method for 2-d self-similar image synthesis," *Image Processing, IEEE Transactions on*, vol. 5, no. 5, pp. 754–761, May 1996.

[9] K. Williams and D. Jackson, "Bistatic bottom scattering: Model, experiments, and model/data comparison," APL-UW, Tech. Rep., 1997.

[10] A. C. Berry, "The accuracy of the gaussian approximation to the sum of independent variates." *Trans. Amer. Math. Soc.*, vol. 49, pp. 122–136, 1941.

[11] Y. Pailhas, "Sonar systems for objects recognition," Ph.D. dissertation, Heriot-Watt University, 2012.

[12] A. Home and G. Yates, "Bistatic synthetic aperture radar," *IEEE RADAR 2002*, pp. 6–10, 2002.